CrossMark

Spectroscopic studies and thermal decomposition for (bis-((*E*)-2-(4-ethylphenylimino)-1,2-diphenylethanone) Schiff base and its Co(II), Ni(II), Cu(II), Zn(II) and Cd(II) complexes prepared by direct and template reactions

Sanaa M. Emam[1] · **Saeyda A. AbouEl-Enein**[1] · **Esam M. Emara**[1]

Abstract A new Schiff base (bis-((*E*)-2-(4-ethylphenylimino)-1,2-diphenylethanone) containing four active coordination centers (ONNO) and its metal complexes have been synthesized and characterized by elemental analyses, spectroscopic methods, molar conductance, thermal and magnetic measurements. The tetrahedral and square planar trinuclear Co(II), Ni(II) and Cu(II) complexes (**1–3**), respectively, have been prepared by direct reaction, while the template reaction gives octahedral complexes (**4–8**) with different stoichiometries 3:1, 2:1, 1:1 (M:L). The ESR spectra of solid copper (II) complexes in powder form showed an axial symmetry with $^{2}B_{1g}$ as a ground state. The thermal decomposition mechanisms of metal complexes were studied. All the thermal decomposition processes ended with the formation of metal oxide. The thermal study showed that the complexes with different solvents of crystallization exercise different types of interaction. The kinetic and thermodynamic parameters have been calculated.

Keywords Benzil · Schiff base · Spectral methods · Thermal studies

Introduction

Schiff bases comprise an important class of organic compounds with a variety of uses; they have been extensively employed as ligands in the formation of transition metal complexes [1]. The chemistry of Schiff base ligands and their metal complexes is very important due to the wide range of applications as antibacterial, antifungal, anticancer and catalytic properties [2–6]. In addition, Schiff base complexes have many applications in biological and industrial systems [7–19]. The tetradentate Schiff base complexes of the first row transition metals can serve as models for some biomolecules, such as Schiff base nickel (II) complexes which have been regarded as models for enzymes such as urease [20, 21]. Benzil (ethanedionediphenyl) and its related compounds have been extensively used as biologically active complexing agents and analytical reagents [22]. It is employed as a selective diketones to obtain macrocycles of desired cavity size and significant reactivity. Metal template condensation often provides selective routes toward products that are not obtainable in the absence of metal ion. Template reactions have been widely used for the synthesis of macrocyclic complexes, in which transition metal ions are generally used as the template agent [23, 24]. In this study, we report on the synthesis and characterization of Co(II), Ni(II) and Cu(II) complexes of the Schiff base ligand derived from 4,4′-methylenedianiline and benzil by direct reactions, but the poor yield problem was facing us in the preparation of some transition and non-transition metal complexes, such as Co(II), Ni(II), Cu(II), Zn(II) and Cd(II), by using template reactions, to overcome this problem. The obtained ligand and its metal complexes were characterized by different analytical, thermal and spectral methods.
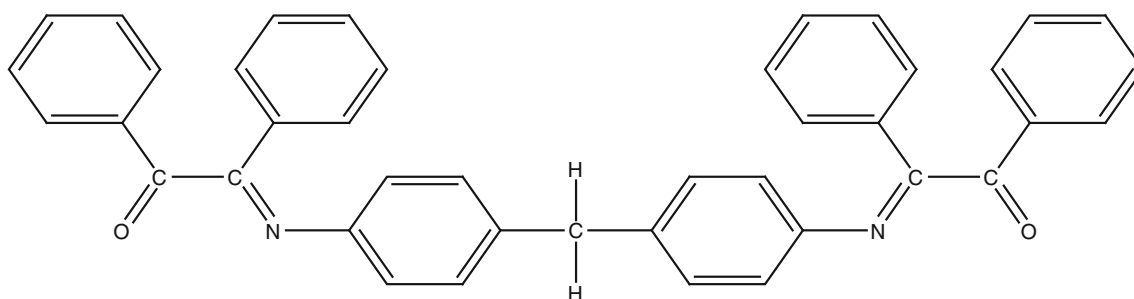
Experimental

Materials and methods

All chemicals were of analytical grade (BDH, Sigma or Aldrich) and were used as received without further purification.

✉ Sanaa M. Emam
  sanaa_drsanaa@yahoo.com

[1] Chemistry Department, Faculty of Science, Menoufia University, Shebin El-Kom, Egypt

Scheme 1 Structure of bis-((*E*)-2-(4-ethylphenylimino)-1,2-diphenylethanone ligand (**L**)

Elemental analyses (C, H and N) were performed on a PerkinElmer 2400 elemental analyzer at Main Defense Chemical Laboratory. Cobalt (II), nickel (II) and copper (II) ions of metal complexes were determined by complexometric titration, whereas zinc (II) and cadmium (II) ions were determined via gravimetric analyses [25].[1] Also, chloride ions were estimated by using Mohr's method ([25], see Footnote 1). Infrared spectra were recorded on a Nicolet FTIR spectrophotometer in the range 4000–400 cm^{-1}. The ^1H NMR spectra were recorded in DMSO-d_6 on a Varian Gemini 200 NMR spectrometer at 300 MHz. Fast atom bombardment (FAB) mass spectrum for the ligand was carried out on a Shimadzu Qp-2010 Plus spectrometer. The electron spin resonance (ESR) spectra were measured on a Varian E-109c spectrometer equipped with a field modulation unit at 100 kHz. Measurements were effected in the X-band frequency 9.71 GHz on a microcrystalline powder at room temperature; the microwave power was around 10 mW. The electronic spectra were measured in Nujol mulls using a PerkinElmer Lambda 4B spectrophotometer. Molar conductivity measurements were taken in DMSO solution 10^{-3} mol L^{-1} using a type CD6N Tacussel conductometer. The thermal analyses (TG/DTG) were carried out by using a Shimadzu DAT/TG-50 thermal analyzer with a heating rate of 10 °C min^{-1} under N_2 atmosphere with a flowing rate of 20 mL min^{-1} from the room temperature up to 900 °C using platinum crucibles. Magnetic susceptibilities were measured at room temperature by a modified Gouy method by using a Johnson Matthey magnetic susceptibility balance. The diamagnetic corrections were calculated using Pascal's constants [26]. The effective magnetic moments were calculated from the equation $\mu_{eff} = 2.84(X_M^{corrt} T)^{1/2}$. Melting points were measured by using Stuart melting point apparatus.

[1] The halide content in the complexes was indirectly determined by Mohr's method after the decomposition of the samples in concentrated nitric acid by boiling, followed by addition of distilled H_2O to give aqueous solution of metal salt. Then, this solution is neutralized by sodium bicarbonate before titration.

Synthesis of Schiff base, bis-((*E*)-2-(4-ethylphenylimino)-1,2-diphenylethanone (L)

A hot ethanolic solution (20 mL) of benzil (20.0 mmol) was added dropwise to a hot ethanol solution (30 mL) of 4,4′-methylenedianiline (10.0 mmol). The reaction mixture was refluxed for 1 h at 50 °C; few drops of concentrated H_2SO_4 were added dropwise to the reactants followed by reflux for 2 h at 70 °C. The formed precipitate was filtered off, washed several times with ethanol and dried in a vacuum desiccator over anhydrous $CaCl_2$ and P_2O_5. The structure of the Schiff base ligand based on elemental analyses and spectral methods is given in Scheme 1.

Synthesis of the Schiff base metal complexes

Complexes (**1–3**) were prepared by direct reaction between the Schiff base ligand (**L**) and Co(II), Ni(II) and Cu(II) chloride salts, while the corresponding Co(II), Ni(II), Cu(II), Zn(II) and Cd(II) chloride complexes (**4–8**) were prepared by template reaction.

Complexes (**1–3**) were synthesized by the addition of (20.0 mmol) of metal chloride dissolved in ethanol to a hot ethanolic solution of (10.0 mmol) of the ligand, and then few drops of triethylamine (TEA) were added to the reactants. The reaction mixture was refluxed for 3 h at 70 °C. The obtained complex was filtered off, washed several times with ethanol and dried in a vacuum desiccator over anhydrous $CaCl_2$ and P_2O_5.

Complexes (**4–8**) were prepared in a similar way to that described above, where (20.0 mmol) of a hot ethanolic solution of benzil was added to (10.0 mmol) of 4,4′-methylenedianiline in 30 mL ethanol. Then, the reaction mixture was stirred for 30 min at 50 °C, and then (20.0 mmol) of appropriate metal chloride in 20 mL ethanol was added dropwise. The reaction mixture was stirred for 30 min in the presence of few drops of concentrated H_2SO_4. The reaction mixture was refluxed for 3 h at 70 °C. The formed complex was filtered off, washed several times with ethanol and dried in a vacuum desiccator

Table 1 The analytical and physical data of Schiff base ligand (**L**) and its metal complexes

No.	Compound	FW	Elemental analyses Found/(Calcd.) %					Λ^a
		Color	C	H	N	Cl	M	
	L	582.71	84.22	5.63	4.52	–	–	–
	$C_{41}H_{30}N_2O_2$	Buff	(84.51)	(5.20)	(4.81)	–	–	
1	$[Co_3(L)Cl_6]\cdot0.5EtOH\cdot7.5H_2O$	1130.66	44.73	4.48	2.32	18.85	15.62	8
	$C_{42}H_{48}N_2O_{10}Co_3Cl_6$	Light brown	(44.62)	(4.28)	(2.48)	(18.84)	(15.64)	
2	$[Ni_3(L)Cl_6]\cdot12.25H_2O$	1192.48	41.75	4.66	2.73	17.94	14.68	13
	$C_{41}H_{54.5}N_2O_{14.25}Ni_3Cl_6$	Light brown	(41.30)	(4.61)	(2.35)	(17.86)	(14.77)	
3	$[Cu_3(L)Cl_6]\cdot6H_2O$	1094.30	44.90	3.86	2.14	19.84	17.32	16
	$C_{41}H_{42}N_2O_8Cu_3Cl_6$	Dark brown	(45.00)	(3.87)	(2.56)	(19.46)	(17.39)	
4	$[Co_3(L)Cl_5(H_2O)_7]\cdot Cl\cdot4.5EtOH$	1305.93	46.47	5.59	2.63	16.52	13.61	59
	$C_{50}H_{71}N_2O_{13.5}Co_3Cl_6$	Blue	(45.99)	(5.48)	(2.50)	(16.31)	(13.54)	
5	$[Ni_2(L)Cl_4(H_2O)_4]\cdot2EtOH$	1006.31	53.98	5.05	3.13	13.87	11.22	12
	$C_{45}H_{50}N_2O_8Ni_2Cl_4$	Yellowish brown	(53.71)	(5.01)	(2.78)	(14.11)	(11.66)	
6	$[Cu_2(L)_2Cl_4]\cdot0.25EtOH\cdot13H_2O$	1680.14	58.89	5.23	3.65	8.55	6.59	24
	$C_{82.5}H_{87.5}N_4O_{17.25}Cu_2Cl_4$	Brown	(58.98)	(5.25)	(3.33)	(8.45)	(7.56)	
7	$[Zn_2(L)_2Cl_4]\cdot13.5H_2O$	1681.39	58.57	5.47	3.32	8.18	7.84	17
	$C_{82}H_{87}N_4O_{17.5}Zn_2Cl_4$	Buff	(58.58)	(5.22)	(3.33)	(8.45)	(7.78)	
8	$[Cd_2(L)_2Cl_4]\cdot0.25EtOH\cdot10.5H_2O$	1732.90	57.71	4.39	2.91	7.98	12.34	29
	$C_{82.5}H_{82.5}N_4O_{14.75}Cd_2Cl_4$	Buff	(57.18)	(4.80)	(3.23)	(8.19)	(12.97)	

^{a} Ω^{-1} cm^2 mol^{-1}

over anhydrous $CaCl_2$ and P_2O_5. The melting point of the ligand is 184 °C.

Results and discussion

Analytical data

All the solid metal complexes are colored, stable at room temperature, non-hygroscopic and partially soluble in most organic solvents, such as chloroform, methanol, ethanol, acetonitrile and DMF, and freely soluble in DMSO. The molar conductance values (8–29 Ω^{-1} cm^2 mol^{-1}) of the metal complexes in DMSO solution (10^{-3} mol L^{-1}) at room temperature (Table 1) revealed that all complexes (except **4**) are non-electrolytes, indicating that chloride ions are directly coordinated to metal ions [27–30, 39], while the value of Co(II) complex (**4**) (59 Ω^{-1} cm^2 mol^{-1}) typified 1:1 electrolyte [27]. The analytical data (Table 1) revealed that the direct reaction method gave complexes (**1**–**3**) with chemical formula $[M_3(L)Cl_6]\cdot m$EtOH$\cdot n$H$_2$O, where M=Co(II), Ni(II) and Cu(II), $m = (0.5, 0, 0)$ and $n = (7.5, 12.25, 6)$, respectively. However, the template reaction (1MDA:2benzil:2metal) produced complexes with different stoichiometries (1L:3M), (1L:2M) and (1L:1M). Co(II) complex (**4**) is formed with chemical formula

$[Co_3(L)Cl_5(H_2O)_7]\cdot Cl\cdot4.5EtOH$, while Ni(II) complex (**5**) has a chemical formula $[Ni_2(L)Cl_4(H_2O)_4]\cdot2EtOH$. Moreover, the sandwich Cu(II), Zn(II) and Cd(II) complexes (**6**–**8**) are formed with chemical formula $[M_2(L)_2Cl_4]$-mEtOH$\cdot n$H$_2$O, where M=Cu(II), Zn(II), Co(II); $m = (0.25, 0, 0.25)$ and $n = (13, 13.5, 10.5)$, respectively.

Mass spectra of Schiff base ligand

Fast atom bombardment mass spectrum (FAB-MS) of the ligand (**L**) was carried out and investigated. The signal appears at $m/z = 582$ amu and is due to the formation of the molecular ion $(C_{41}H_{30}N_2O_2)^+$ for the ligand. This confirms the proposed formula and agrees well with the elemental analyses for the ligand.

Infrared spectra

The infrared spectrum of the Schiff base ligand (Table 2) lists the most useful assignments for bands diagnostic to the mode of coordination of the ligand. The spectrum of the ligand (Fig. 1) displays the fundamental bands of aromatic rings v(CH), ring bending, p-disubstituted and monosubstituted benzene rings deformation characterized by 3065, 1509, (864, 814) and 761 cm^{-1}, respectively [30–34]. While the bands at 1325 and 1073 cm^{-1} are due to the in-

Table 2 Infrared spectral bands (cm^{-1}) of Schiff base ligand and its metal complexes and their assignments

No.	Compound	ν(OH) H$_2$O/EtOH	ν(C=O)	ν(C=C) + ν(C=N)	ν(N-ph)	p-Disubstituted benzene ring	δ(C=O)	γ(C=O) + ν(M-O)	ν(M-N)
	L	3585 (vw) 3454 (m)	1672 (m)	1603 (w,sp) 1564 (w,sp)	1325 (m)	864 (m) 814 (W)	691 (w)	636 (w) 605 (m)	–
1	[Co$_3$(L)Cl$_6$]·0.5EtOH·7.5H$_2$O	3592 (m) 3333 (m)	1671 (w)	1623 (w) 1586 (m)	1321 (w)	871 (w) 830 (m)	660 (m)	– 586 (m)	521 (w)
2	[Ni$_3$(L)Cl$_6$]·12.25H$_2$O	3327 (m)	1671 (w,br)	1620 (w) 1582 (m)	1317 (w)	873 (m) 829 (m)	660 (m)	– 591 (m)	524 (w)
3	[Cu$_3$(L)Cl$_6$]·6H$_2$O	3449 (w) 3364 (vw)	1681 (sh)	1626 (w,sp) 1597 (w,sp)	1321 (w)	872 (w) 827 (w)	653 (m)	617 (w) 590 (w)	514 (w)
4	[Co$_3$(L)Cl$_5$(H$_2$O$_7$]·Cl·4.5EtOH	3324 (m) 3244 (s)	1667 (w)	1586 (s) –	1305 (v,w)	869 (m) 823 (m)	714 (m)	648 (s) 581 (s)	520 (w)
5	[Ni$_2$(L)Cl$_4$(H$_2$O)$_4$]·2EtOH	3316 (m) 3259 (m)	1667 (s)	1615 (w) 1577 (s)	1318 (m)	870 (s) 818 (m)	692 (m)	652 (s) 584 (s)	524 (w)
6	[Cu$_2$(L)$_2$Cl$_4$]·0.25EtOH·13H$_2$O	3302 (s) 3232 (s)	1670 (m)	1608 (w) 1570 (m)	1324 (w)	869 (m) 819 (m)	687 (m)	619 (m) 578 (m)	503 (w)
7	[Zn$_2$(L)$_2$Cl$_4$]·13.5H$_2$O	3296 (m) 3250 (s)	1677 (w)	1589 (m) 1554 (w)	1315 (w)	861 (m) 816 (s)	688 (m)	631 (w) 611 (s) 574 (s)	524 (m)
8	[Cd$_2$(L)$_2$Cl$_4$]·0.25EtOH·10.5H$_2$O	3314 (s) 2245 (m)	1664 (m)	1611 (m) 1571 (w,sp) 1553 (w,sp)	1310 (m)	864 (m) 814 (s)	690 (m)	609 (s) 578 (s)	523 (w)

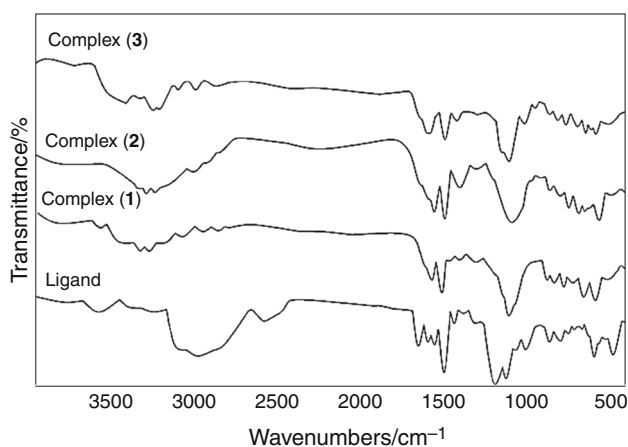*vw* Very weak, *w* weak, *m* medium, *s* strong, *b* broad, *sh* shoulder, *sp* splitted

Fig. 1 IR spectra of the ligand, $[Co_3(L)Cl_6]\cdot0.5EtOH\cdot7.5H_2O$ (**1**), $[Ni_3(L)Cl_6]\cdot12.25H_2O$ (**2**) and $[Cu_3(L)Cl_6]\cdot6H_2O$ (**3**)

plane CH deformation of phenyl ring and v(N-phenyl) [32], also the bands at 2927, 1449, 1189, 1121 and 761 cm^{-1} are due to stretching, scissoring, wagging, twisting and rocking vibration modes of methylene group, respectively [32]. The spectrum shows weak and medium bands at 1672 and (1603, 1564 cm^{-1}) assignable to v(C=O) [35–37] and stretching vibration of azomethine groups including the v(C=C) of benzene rings, respectively [31, 38]. The weak nature of these bands may be due to the combination of aromatic v(C=C) bands. The spectrum shows bands at 691 and (636, 605 cm^{-1}) due to δ(C=O) and γ(C=O), respectively. This confirms the presence of carbonyl group in the skeleton of the ligand.

The spectra of complexes (**1–3**) reveal that the medium v(C=O) ligand band (1672 cm^{-1}) showed a change in its shape and position (Fig. 1). On the other hand, the δ(C=O) ligand band (691 cm^{-1}) shifted to lower values via (31–38 cm^{-1}), whereas the weak γ(C=O) (636 cm^{-1}) was absent in Co(II) and Ni(II) complexes and shifted to lower frequency by 19 cm^{-1} in Cu(II) complex (Table 2). While the second γ(C=O) ligand band (605 cm^{-1}) appeared as a strong feature in complexation to suggest its combination v(M–O) [30, 39–41], the v(C=N) ligand band (1564 cm^{-1}) shifted to higher frequency by (18–33 cm^{-1}) in metal complexes (**1–3**) with the appearance of new weak bands in range (514–524 cm^{-1}) which are suggested to v(M–N) [7, 30, 42, 43]. According to the above arguments, the ligand binds with the metal ions via carbonyl oxygen and azomethine nitrogen atoms. It was noted that v(N–phenyl), CH$_2$ rocking and p-disubstituted benzene ring bands (Table 2) suffered change in shape and position upon complexation. This consideration supported another evidence for the participation of the nitrogen atom of the azomethine groups in chelation.

The spectra of complexes (**4–8**) which were prepared by template reaction display bands at ranges (1664–1677),

(687–714), (609–652) and (574–584 cm^{-1}) assignable to v(C=O), δ(C=O), γ(C=O) and v(M–O), respectively [30, 35–38, 40]. The spectra of benzil and the prepared Schiff base ligand showed γ(C=O) at (636–639) and 605 cm^{-1}. The first band undergoes red/blue shift by (12–26) and (5–27 cm^{-1}), respectively, whereas the second one displayed shift to lower frequency at (21–31 cm^{-1}) upon complexation. This indicates participation of the oxygen atoms of carbonyl groups of benzil moiety in coordination [30, 40, 41].

The different modes of vibration of NH$_2$ were disappeared with the appearance of two bands at (1586–1615) and (1553–1577 cm^{-1}) ranges, due to v(C=N) which corresponding to bands at 1564 and 1603 cm^{-1} in the prepared ligand [7, 38]. It is obvious from comparing the v(C=N) band of the free ligand with that of the metal complexes, the first band showed blue/red shift by (14–17) and (5–12 cm^{-1}) upon complexation with Co(II), Ni(II), Zn(II) and Cu(II) salts, respectively, whereas the second band disappeared in Co(II) complex (**4**) and showed slight shift with Ni(II), Cu(II) and Zn(II) complexes. The spectrum of Cd(II) complex (**8**) showed v(C=N) as a splitted band with negative shift at (11–32 cm^{-1}). The above observation suggests that the nitrogen atom of azomethine groups involved in chelation, and this also supported by the appearance of band in range (503–524 cm^{-1}), assignable to v(M–N) [30, 42, 43]. In addition to carbonyl and azomethine bands, the spectra of complexes gave bands corresponding to CH vibrations of aromatic rings and methylene group [31, 32]. This indicates that the complexes contain MDA and benzil moieties. The above arguments point to that the condensation takes place in presence of metal and few drops of concentrated H$_2$SO$_4$ with the formation of metal complexes.

## ^{1}H NMR of Schiff base and metal complexes (7, 8)

^{1}H NMR spectrum of the Schiff base ligand in DMSO-$d6$ reveals multiple signals at δ (6.84–7.23 ppm) assigned to protons of aromatic rings [40, 43], while the singlet signal at δ 3.83 ppm is due to –CH$_2$ protons. The spectra of Zn(II) and Cd(II) complexes (**7**, **8**) show the resonance of aromatic protons in range δ (6.35–6.94 ppm) and –CH$_2$ signal at δ (3.62–3.65 ppm), respectively, which considered upfield shift compared to free ligand. This observation confirms the IR discussion which suggests that the aromatic rings strongly affected upon chelation.

Molecular modeling study of the Schiff base ligand

Molecular modeling studies using (MM$^+$) calculations [44–46] are performed to determine a better understanding of geometrical structure of the investigated ligand. The

Table 3 Important bond lengths characterized for Schiff base ligand

Bond	Bond length/Å	Bond	Bond length/Å
C(4)–N(14)	1.2601	C(18)–C(16)	1.3510
C(8)–N(15)	1.2600	C(17)–C(19)	1.3510
N(14)=C(16)	1.2600	C(18)=O(44)	1.2079
N(15)=C(17)	1.2600	C(19)=O(45)	1.2080
C(18)–C(32)	1.3510	C(19)–C(33)	1.3510
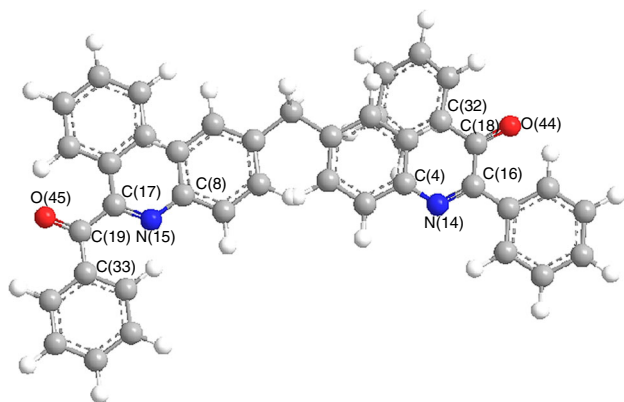
Fig. 2 Molecular modeling for Schiff base ligand

molecular mechanisms (MM$^+$) have enormous applications in the field of coordination chemistry [45, 46]. The molecular modeling of the ligand, Table 3 and Fig. 2, showed some of the important bond lengths and numbering of the ligand Skelton. It was observed that the stability order decreases in this direction:

C(18)=O(44) $\approx$ C(19)=O(45) > N(14)=C(16) $\approx$ N(15)=C(17) > C(4)–N(14) $\approx$ C(8)–N(15) > C(16)–C(18) $\approx$ C(17)–C(19) $\approx$ C(19)–C(35)

Electronic spectra and magnetic moments

The tentative assignments of the significant electronic spectral bands of the Schiff base ligand (L) and its metal complexes in Nujol mulls are presented in Table 4. The electronic spectrum of the ligand (L) exhibits three strong absorption maxima at 252, 296 and 328 nm which are assigned to electronic transitions between bonding and anti-bonding orbitals ($\pi - \pi^*$) of phenyl rings as well as carbonyl and azomethine groups [47–49]. In addition to these, two low intense bands appear at 468 and 515 nm due to the electronic transitions from the lone pair of electrons on the heteroatom nitrogen of (C=N) to the anti-bonding π^* orbital and ($n - \pi^*$) electronic transitions of the entire conjugate system of the ligand [30]. In metal complexes, the $\pi - \pi^*$ transition of the phenyl ring shifts slightly and remains almost constant, whereas the $\pi - \pi^*$ and $n - \pi^*$ of (C=N) and (C=O) groups shift toward lower frequency

due to the change in the electron density of the ligand upon complexation [48, 49]. Also, the spectra of metal complexes show bands at 483–510 nm which may be attributed to ligand to metal charge transfer (LMCT) and Cl → M charge transfer transitions [50–54]. These shifts of bands indicate to bonding of the ligand to the metal ions.

The geometry of metal complexes has been observed from electronic spectra and their magnetic moment values. The spectrum of Co(II) complex (**1**) displays high intense band at 700 nm and a shoulder band at 644 nm assigned to $^4A_2(F) \rightarrow {}^4T_1(F)$ (υ_2) and $^4A_2(F) \rightarrow {}^4T_1(P)$ (υ_3) transition, respectively. This confirms tetrahedral structure for cobalt (II) complexes [55, 56, 66]. Cobalt (II) complex (**4**) exhibits three bands located at 630, 580 and 515 nm characterized to $^4T_{1g}(F) \rightarrow {}^4T_{2g}(F)$ (υ_1), $^4T_{1g}(F) \rightarrow {}^4A_{2g}(F)$ (υ_2) and $^4T_{1g}(F) \rightarrow {}^4T_{1g}(P)$ (υ_3) transitions, respectively. This supports high-spin octahedral geometry around cobalt (II) ion [57–61]. The magnetic moment values for complexes (**1**, **4**) (Table 4) are gathered with the d–d electronic transitions to suggest the tetrahedral and octahedral geometry for complexes (**1**,**4**), respectively [55–61]. The lower magnetic moment values (3.84, 4.1 BM) for Co(II) complexes (**1**,**4**) indicate anti-ferromagnetic coupling of spins of Co(II) ions.

The nickel (II) complex (**2**) shows one band at 693 nm which may be attributed to $^3T_1(F) \rightarrow {}^3T_1(P)$ transition indicating tetrahedral geometry around Ni(II) ion, and this is confirmed by its magnetic moment value (2.98 BM) [57, 62, 65–67]. The electronic spectrum of Ni(II) complex (**5**) exhibits two bands at (800, 710) and 462 nm ascribed to $^3A_{2g}(F) \rightarrow {}^3T_{1g}(F)$ (υ_2) and $^3A_{2g}(F) \rightarrow {}^3T_{1g}(P)$ (υ_3) transitions, respectively. The υ_2 transition appears as doublet; this is due to the forbidden transition to ^1E_g level that interacts with $^3T_{1g}(F)$ level and also due to spin–orbit coupling [56]. These transitions and magnetic moment value (3.49 BM) are consistent with octahedral structure of nickel (II) ion [30, 61–63].

[Cu$_3$(L)Cl$_6$]·6H$_2$O complex (**3**) have two bands at 690 and 556 nm for $^2B_{1g} \rightarrow {}^2E_g$ and $^2B_{1g} \rightarrow {}^2A_{1g}$ electronic transitions, respectively, and the magnetic moment value (0.8 BM) is typified with square planar structure around Cu(II) ions [52–54, 61–63, 65]. Moreover, the electronic spectrum of Cu(II) complex (**6**) showed two bands at 694 and 584 nm and assigned to $^2B_{1g} \rightarrow {}^2B_{2g}$ and $^2B_{1g} \rightarrow {}^2E_g$, respectively. The magnetic moment value for this complex (1.56 BM) is gathered with the d–d transitions to establish the distorted octahedral geometry [30, 48, 50, 51, 61, 64]. The relatively low values of magnetic moment of complexes (**1**–**6**) indicate the metal–metal interaction [53, 54].

The proposed chemical structures for the synthesized metal complexes (based on elemental analyses and spectral methods) are represented in Scheme 2.

**Table 4** Electronic spectral data and magnetic moment values of Schiff base ligand and its metal complexes

No.	Compound	Electronic spectral bands/nm	Assignments	$\mu_{eff.}$ (BM) (per metal ion)
	L	468, 515	$n - \pi^*$	–
		252,296,328	$\pi - \pi^*$	–
1	$[Co_3(L)Cl_6] \cdot 0.5EtOH \cdot 7.5H_2O$	700	$^4A_2(F) \rightarrow {}^4T_1(F)$	3.84
		644	$^4A_2(F) \rightarrow {}^4T_1P)$	
		428,468,512	LMCT	
		252,296,312	Intraligand transition	
2	$[Ni_3(L)Cl_6] \cdot 12.25H_2O$	693	$^3T_1(F) \rightarrow {}^3T_1(P)$	2.98
		434,510	LMCT	
		250,289,310	Intraligand transition	
3	$[Cu_3(L)Cl_6] \cdot 6H_2O$	690	$^2B_{1g} \rightarrow {}^2E_g$	0.80
		556	$^2B_{1g} \rightarrow {}^2A_{1g}$	
		434,476,514	LMCT	
		254,292,320	Intraligand transition	
4	$[Co_3(L)Cl_5(H_2O)_7] \cdot Cl \cdot 4.5EtOH$	630	$^4T_{1g}(F) \rightarrow {}^4T_{2g}(F)$	4.1
		580	$^4T_{1g}(F) \rightarrow {}^4A_{2g}(F)$	
		515	$^4T_{1g}(F) \rightarrow {}^4T_{1g}(P)$	
		483	LMCT	
		252,286,316	Intraligand transition	
5	$[Ni_3(L)Cl_4(H_2O)_4] \cdot 2EtOH$	800,710	$^3A_{2g}(F) \rightarrow {}^3T_{1g}(F)$	3.49
		462	$^3A_{2g}(F) \rightarrow {}^3T_{1g}(P)$	
		445,504	LMCT	
		245,279,328	Intraligand transition	
6	$[Cu_2(L)_2Cl_4] \cdot 0.25EtOH \cdot 13H_2O$	694	$^2B_{1g} \rightarrow {}^2B_{2g}$	1.56
		584	$^2B_{1g} \rightarrow {}^2E_g$	
		468,502	LMCT	
		252,288,312	Intraligand transition	
7	$[Zn_2(L)_2Cl_4] \cdot 13.5H_2O$	428,468,506	LMCT	Diamagnetic
		252,296,319	Intraligand transition	
8	$[Cd_2(L)_2Cl_4] \cdot 0.25EtOH \cdot 10.5H_2O$	432,468,506	LMCT	Diamagnetic
		252,296,319	Intraligand transition	

Thermal studies

The thermoanalytical data describe the thermal decomposition pathway of metal complexes, give simulations about the decomposition mechanism and identify the different types of solvent of crystallization. Thermal behavior of the ligand and its metal complexes has been studied by using TG and DTG analyses, and the results are listed in Table 5 and represented in Fig. 3.

The TG curve pattern of the ligand ($C_{41}H_{30}N_2O_2$) reveals that the thermal stability is up to 184 °C, and insignificant mass loss (0.6 %) below 100 °C caused by evaporation of residual solvent (0.25 H_2O) from the sample. The TG and DTG curves profile indicates that the thermal decomposition of the ligand comprises of mainly three steps within (184–270), (270–381) and (381–872 °C)

temperature ranges (Table 5). The decomposition starts with the elimination of two carbonyl groups, and this was confirmed with the disappearance of the carbonyl group stretching from infrared spectrum of the arrested material after heated up to 270 °C (Fig. 4). The modeling structure of the ligand (Fig. 2; Table 3) shows that the C(16)–C(18), C(17)–C(19), C(19)–C(35) and C(18)–C(32) bonds are more lengthen than the other bonds; this is another evidence of the suggested mechanism for the starting thermal decomposition pathway for the ligand (Scheme 3). This step is followed by loss of three phenyl moieties ($C_{18}H_{12}$). The first and second steps are characterized by well-defined DTG peaks at ($T_{max} = 228, 328$ °C), respectively, and proceed in a sharp temperature range, and this reveals that the mass loss process proceeds fast. After that, the decomposition of the rest organic material occurs smoothly

Scheme 2 Structure of Schiff
base title metal complexes
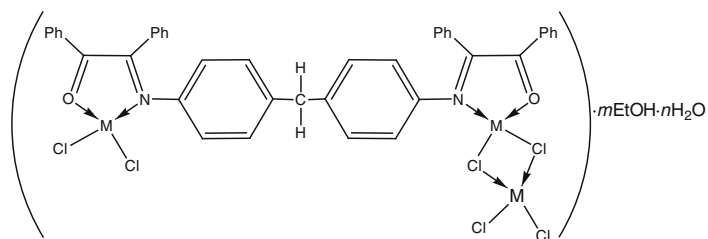
Structure of metal complexes (1, 2)

Complex	M	m	n
1	Co	0.5	7.5
2	Ni	0	12.25
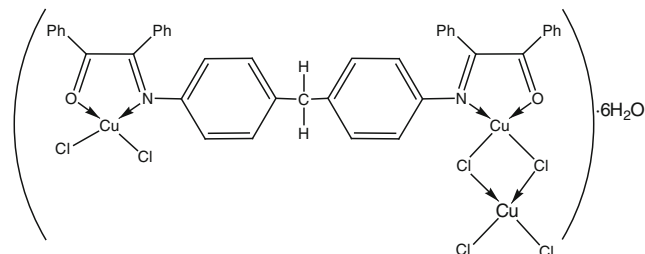
Structure of Cu(II) complex (3)
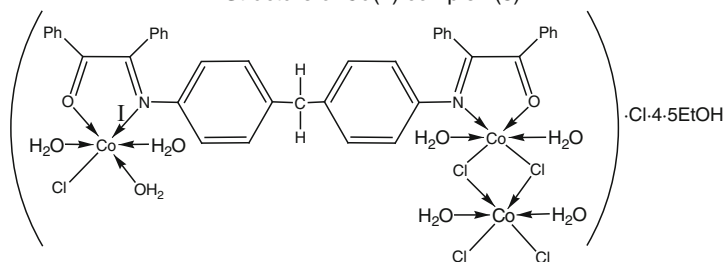
Structure of Co(II) complex (4)

where Ph =
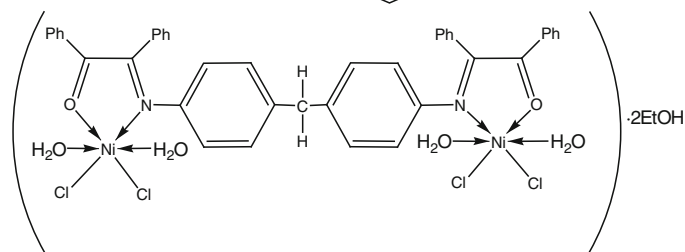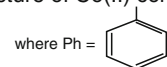
Structure of Ni(II) complex (5)
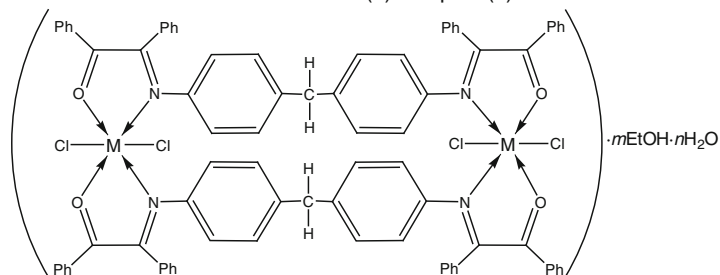
Complex	M	m	n
6	Cu	0.25	13
7	Zn	0	13.5
8	Cd	0.25	10.5

Table 5 Thermal decomposition of Schiff base ligand and its metal complexes

No.	Compound	TG range Temperature/°C	DTG peak Temperature/°C	Mass loss/% Found	Calcd.	Assignment	T_S Temperature/°C
	L·0.25H$_2$O	26–184	55[f]	0.60	0.78	Loss of 0.25 mol of H$_2$O[a]	184
		184–270	228[h]	9.26	9.54	Loss of 2CO[d]	
		270–381	328[f]	38.67	38.88	Loss of C$_{18}$H$_{12}$[d]	
		381–872	660[h]	50.57	49.79	Loss of C$_{20.5}$H$_{18}$N$_2$[d]	
		At 872		0.75	1.02	0.5C[r]	
1	[Co$_3$(L)Cl$_6$]·0.5EtOH·7.5H$_2$O	26324	39[f]	10.68	10.80	Loss of 0.5 mol of EtOH and 5.5 mol of H$_2$O[a+b]	324
			73[f]				
			166[h]				
		324–582	455[r]	51.83	51.96	Loss of C$_{27}$H$_{22}$N$_2$ and 3Cl$_2$[d]	
		582–652	–	–	–		
		652–810	746[e]	6.58	6.38	Loss of 5C and 6H$_2$[d]	
		810–839	–	–	–	–	
		839–897	879[f]	2.29	2.12	Loss of 2C[d]	
		At 897		28.62	28.73	Co$_3$O$_4$ + 7C[r]	
2	[Ni$_3$(L)Cl$_6$]·12.25H$_2$O	26–369	43[e]	15.31	15.11	Loss of 10 mol of H$_2$O[a]	369
		369–588	442[r]	51.18	51.15	Loss of C$_{27}$H$_{22}$N$_2$, 1.25 mol of H$_2$O and 3Cl$_2$[d]	
		588–641	–	–	–	–	
		641–899	691[f]	5.23	5.63	Loss of 4.75C and 5H$_2$[d]	
		At 899		28.28	28.11	3NiO + 9.25C[r]	
3	[Cu$_3$(L)Cl$_6$]·6H$_2$O	23–222	44[f]	4.18	4.12	Loss of 2.5 mol of H$_2$O[a]	222
		222–283	253[c]	27.94	27.92	Loss of C$_{21}$H$_{15}$N$_2$ and 0.5 mol of H$_2$O[d]	
		283–379	332[c]	34.65	34.65	Loss of 13C, 5H$_2$ and 3Cl$_2$[d]	
		379–450	409[f]	2.26	2.47	Loss of 1.5 mol of H$_2$O[d]	
		450–600	–	–	–	–	
		600–898	679[f]	4.69	4.77	Loss of 3C, 3.5H$_2$ and 0.5H$_2$O[d]	
		At 898		26.28	26.17	3CuO + 4C[r]	
4	[Co$_3$(L)Cl$_5$(H$_2$O)$_7$]·Cl·4.5EtOH	23–193	39[g]	5.64	5.29	Loss of 1.5 mol of EtOH[b]	350
			157[e]				
		193–350	333[c]	7.34	7.21	Loss of 1.25 mol of EtOH and 0.5Cl$_2$[b]	
		350–561	399[c]	55.55	55.34	Loss of C$_{27}$H$_{22}$N$_2$, 5 mol of H$_2$O, 1.75 mol of EtOH and 2.5Cl$_2$[d]	
			509[e]				
		561–899	743[h]	6.80	7.74	Loss of 7.5C and 6.0 H$_2$[d]	
		At 899		24.66	24.42	Co$_3$O$_4$ + 6.5C[r]	
5	[Ni$_2$(L)Cl$_4$(H$_2$O)$_4$]·2EtOH	25–327	40[g]	9.09	9.16	Loss of 2 mol of EtOH[b]	327
			170[f]				
		327–499	436[r]	58.48	58.49	Loss of C$_{27}$H$_{22}$N$_2$, 4 mol of H$_2$O and 2Cl$_2$[d]	
		499–719	517e	15.67	15.72	Loss of 12.5 C and 4H$_2$[d]	
			685g				
		At 719		16.76	16.63	2NiO + 1.5C[r]	
6	[Cu$_2$(L)$_2$Cl$_4$]·0.25EtOH·13H$_2$O	22–237	45[f]	10.99	10.87	Loss of 0.25 mol of EtOH and 9.5 mol of H$_2$O[a+b]	237
			164[f]				
			182[f]				
			203[g]				
			220[g]				
		237–391	267[h]	19.75	19.79	Loss of C$_{26}$H$_{20}$[d]	
			360[f]				
		391–703	458[e]	59.87	59.87	Loss of C$_{56}$H$_{40}$N$_4$O$_2$, 2Cl$_2$ and 3.5 mol of H$_2$O[d]	
			666[h]				
		At 703		9.38	9.46	2CuO[r]	

Table 5 continued

No.	Compound	TG range Temperature/°C	DTG peak Temperature/°C	Mass loss/% Found	Mass loss/% Calcd.	Assignment	T_S Temperature/°C
7	$[Zn_2(L)_2Cl_4]\cdot13.5H_2O$	25–283	51[f]	14.07	14.47	Loss of 13.5 mol of H_2O[a]	283
			176[e]				
			254[e]				
		283–376	358[c]	19.88	19.77	Loss of $C_{26}H_{20}$[d]	
		376–675	452[c]	54.82	54.66	Loss of $C_{54}H_{40}N_4O_2$ and $2Cl_2$[d]	
			610[f]				
			652[f]				
			At 675	11.23	11.10	$2ZnO + 2C$[r]	
8	$[Cd_2(L)_2Cl_4]\cdot0.25EtOH\cdot10.5H_2O$	28–277	139[e]	10.37	10.02	Loss of 0.25 mol of EtOH and 9 mol of H_2O[a+b]	277
			245[e]				
		277–364	325[c]	19.76	19.70	Loss of $C_{26}H_{20}$ and 0.5 mol of H_2O[d]	
		364–896	431[c]	55.46	55.46	Loss of $C_{56}H_{40}N_4O_2$, $2Cl_2$ and one mol of H_2O[d]	
			587[c]				
			At 896	14.41	14.82	$2CdO$[r]	

[a] Dehydration

[b] Desolvation

[c] Strong

[d] Decomposition

[e] Medium

[f] Weak

[g] Very weak

[h] Broad

r: Final redidue

within the gradually over wide temperature range, suggesting that the decomposition proceeds slowly. The estimated total mass loss for the ligand is consistent with the calculated total mass loss at the observed decomposition steps within temperature range (26–872 °C) as shown in Table 5.

The isostructural trinuclear $[Co_3(L)Cl_6]$-0.5EtOH·7.5H$_2$O complex (**1**) and $[Ni_3(L)Cl_6]\cdot12.25H_2O$ complex (**2**) largely exhibit the similar thermal behavior, indicating isothermal character at room temperature. The TG curves showed mass loss in range (26–369 °C), assigned to complete desolvation and partial dehydration. After that, the TG curves display mass loss in range (51.18–51.83 %) within range (324–588 °C) (Table 5), corresponding to thermal degradation of the most part of the ligand (release of bis-((E)-N-benzylidenebenzenamine) along with dechlorination ($C_{27}H_{22}N_2 + 3Cl_2$). This process was associated with strong broad DTG peaks at ($T_{max} = 455$, 442 °C) for Co(II) and Ni(II) complexes, respectively, suggesting the overlapping of more than one decomposition process. This is obviously clear from the DTG curve of Co(II) complex (**1**) which recorded under atmospheric air and gave the same decomposition products obtained under N_2 atmosphere as shown in Fig. 3. The TG

curves show some stability within range (582–652 °C) and then followed by successive small mass loss leading to the formation of ($Co_3O_4 + 7C$) and ($3NiO + 9.25C$) as final products [34, 67]. The X-ray diffraction pattern (XRD) of the obtained ($Co_3O_4 + 7C$) (Fig. 5) was confirmed with ASTM card number (3-65-3103) and infrared spectrum of the final residue (Fig. 6) which shows two bands at (649.47, 548.89 cm^{-1}), assigned to v(M–O) [7, 41]. It is obviously clear that the final residues resulted from the decomposition of Co(II) complex (**1**) under nitrogen or atmospheric air and Ni(II) complex (**2**) are evident that the oxygen atoms of the ligand as well as lattice water molecules are responsible for the formation of metal oxide; two or one molecule of lattice water contributed in the formation of ($Co_3O_4 + 7C$) or ($3NiO + 9.25C$), respectively.

The trinuclear square planar $[Cu_3(L)Cl_6]\cdot6H_2O$ complex (**3**) has thermal decomposition pattern that differs from that of Co(II) and Ni(II) complexes (**1**, **2**). The estimated TG mass loss (4.18 %) up to 222 °C is reasonable for the removal of 2.5 mol of H_2O. The rest of H_2O molecules are associated with the decomposition of the material [68]. The DTG curve displays well-defined splitted peaks at ($T_{max} = 253$, 332 °C); those two peaks refer to two subsequent decomposition processes. The TG curve shows

Fig. 3 TG/DTG curves of the Schiff base ligand and its metal complexes
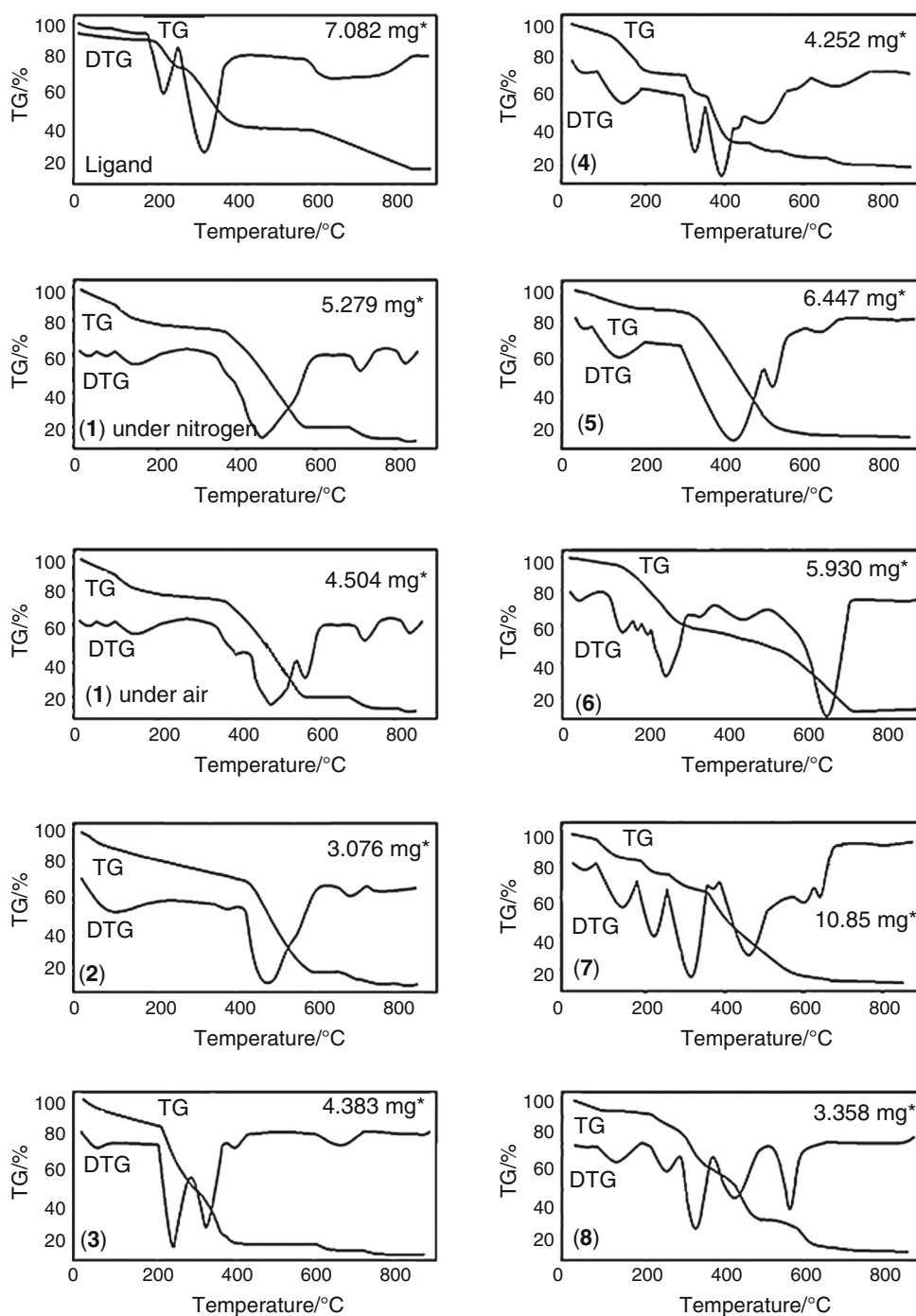
*: Mass of sample

sharp decomposition at 222 °C with mass loss 27.94 % up to 283 °C, corresponding to elimination of ($C_{21}H_{15}$-$N_2 + 0.5H_2O$), and then followed by TG mass loss 34.65 % up to 379 °C, consistent with the removal of ($13C + 5H_2 + 3Cl_2$). The last step was associated with small mass loss (2.26 %) and weak DTG peak at $T_{max} = 409$ °C, due to loss of 1.5 mol of H_2O. The TG

curve displays no mass loss up to 600 °C. After that, it undergoes mass loss (4.69 %) at $T_{max} = 679$ °C, leaving $3CuO + 4C$ as a final product [30, 34, 65–67].

The TG curve of the octahedral [$Co_3(L)Cl_5(H_2O)_7$]-$Cl·4.5EtOH$ complex (**4**) displays mass loss (5.64 %) up to 193 °C, assigned to the removal of 1.5 mol of EtOH, followed by TG mass loss (7.34 %) at ($T_{max} = 333$ °C) up to 350 °C,
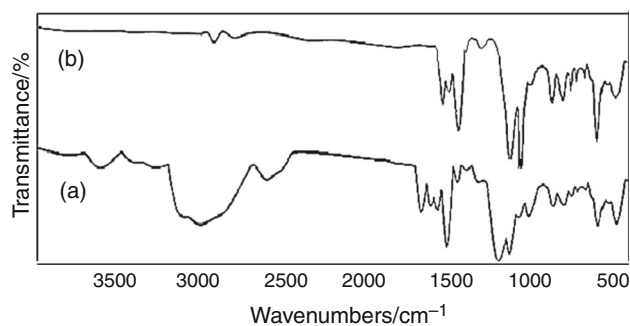
Fig. 4 IR spectrum of the Schiff base ligand after heated up to 270 °C. *a* Before heating; *b* after heating

Fig. 5 XRD pattern of Co_3O_4 as a final product of the thermal decomposition of Co(II) complex (**1**)

equivalent to elimination of (ionic chloride + 1.25EtOH) (Table 5). After that, the thermal decomposition begins at 350 °C; the DTG curve displays a strong broad peak at ($T_{max} = 399$ °C) associated with a medium one at ($T_{max} = 509$ °C). This step was associated with TG mass loss (55.55 %) up to 561 °C, corresponding to the removal of ($C_{27}H_{22}N_2$ + 5 mol of H_2O + 1.75 mol of EtOH + 2.5Cl_2). After that, the TG curve profile shows a small mass loss (6.80 %) up to 899 °C at $T_{max} = 743$ °C (Table 5). Finally, the TG curve of this complex shows complete decomposition

for the organic ligand ended with the formation of (Co_3O_4 + 6.5C) as a final product [67]. The X-ray diffraction pattern (XRD) of the obtained (Co_3O_4 + 6.5C) (Fig. 7) was confirmed with ASTM card number (3-65-3103) [67] and infrared spectrum of the final residue (Fig. 8) which shows two bands at (650, 539 cm^{-1}), attributed to ν(M–O) [7, 41].

The TG curve profile of binuclear octahedral Ni(II) complex (**5**) [$Ni_2(L)Cl_4(H_2O)_4$]·2EtOH has the same thermal decomposition behavior of trinuclear Co(II) and Ni(II) complexes (**1,2**), with the exception of releasing water of crystallization. The TG curve displays mass loss (9.09 %)

Scheme 3 Proposed thermal decomposition mechanism for Schiff base ligand

Fig. 6 IR spectrum of Co_3O_4 as a final product of the thermal decomposition of Co(II) complex (**1**)

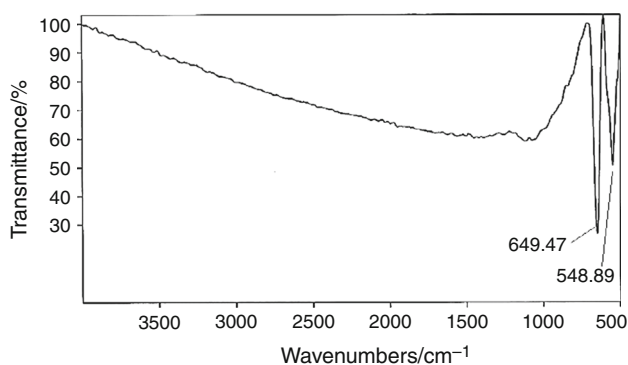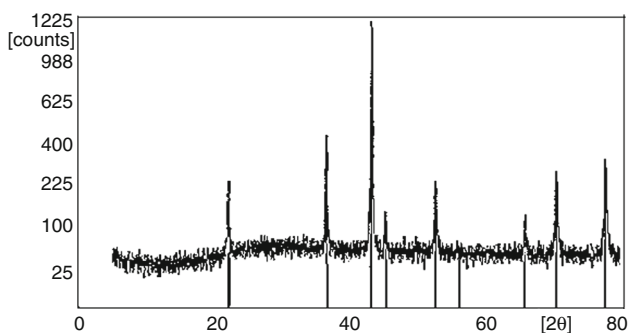**Fig. 7** XRD pattern of Co_3O_4 as a final product of the thermal decomposition of Co(II) complex (**4**)
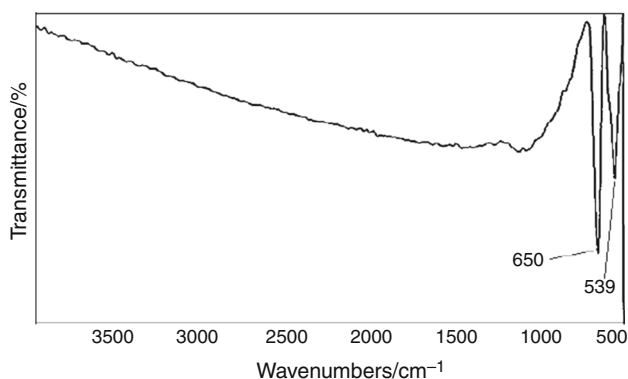

**Fig. 8** IR spectrum of Co_3O_4 as a final product of the thermal decomposition of Co(II) complex (**4**)

up to 327 °C, corresponding to complete desolvation. This step is followed by TG mass loss (58.48 %) up to 499 °C with ($T_{max} = 436$ °C), consistent with the removal of ($C_{27}H_{22}N_2 + 4$ mol of $H_2O + 2Cl_2$) (Table 5). This step is followed by TG mass loss (15.67 %) up to 719 °C with DTG peaks at ($T_{max} = 517$ and 685 °C), due to elimination of ($12.5C + 4H_2$ gas). The thermal decomposition pattern ended with the formation of ($2NiO + 1.5C$) as a final product [34].

According to the above arguments, the trinuclear tetrahedral Co(II), Ni(II) complexes (**1**, **2**), trinuclear octahedral Co(II) complex (**4**) and binuclear octahedral Ni(II) complex (**5**) start thermal decomposition by breaking bonds between coordinated nitrogen atoms and the metal along with the C–C bond of benzil moiety and dechlorination. The metal still bonded with oxygen atoms of carbonyl groups of the ligand and some of lattice or coordinated water to produce metal oxides contaminated with carbon as final products. The thermal decomposition mechanism of Co(II) complex (**1**) is shown in Scheme 4, as an example for the above-mentioned complexes.

The TG and DTG curves profile of Cu(II), Zn(II) and Cd(II) complexes (**6–8**) indicates that they have nearly similar thermal decomposition pathway. It is obvious from the curves that the dehydration and/or desolvation process takes place into two steps. However, the rest of the H_2O molecules are lost along with the decomposition process as indicating from TG mass loss (Table 5). After that, the decomposition of Cu(II), Zn(II) and Cd(II) complexes begins at 237, 283 and 277 °C, respectively. The thermal degradation processes completed through two continuous steps, and all ended with the formation of metal oxide as a final product [30, 34, 65–67]. The first decomposition step of Cu(II), Zn(II) and Cd(II) complexes is characterized by DTG peaks at $T_{max} = (267,360, 358$ and 325 °C) with estimated mass losses 19.75, 19.88 and 19.76 %, respectively. Those mass losses are equivalent to the removal of two molecules of unstable diphenylmethane moieties ($C_{26}H_{20}$), leaving two molecules of unstable octahedral sandwich complexes. This is followed by TG mass loss 59.87, 54.82 and 55.46 % for Cu(II), Zn(II) and Cd(II) complexes, respectively, assignable to pyrolysis of the rest of the organic material as well as the release of two mol of chlorine gas, in addition to the removal of the rest of the H_2O molecules in case of Cu(II) and Cd(II) complexes. The X-ray diffraction pattern (XRD) of the obtained residue (2CuO) (Fig. 9) was confirmed with ASTM card number (89-2531). According to the above thermal decomposition data, the sandwich complexes (**6–8**) start decomposition with the removal of two mol of diphenylmethane followed by dechlorination as well as the decomposition of the five membered chelate ring with the formation of metal oxide. The proposed thermal decomposition mechanism for complexes (**6–8**) is represented in Scheme 5.

Kinetic and thermodynamic studies

The thermodynamic and kinetic parameters of the ligand and its metal complexes were calculated [30, 69, 70, 71] and collected in Table 6.
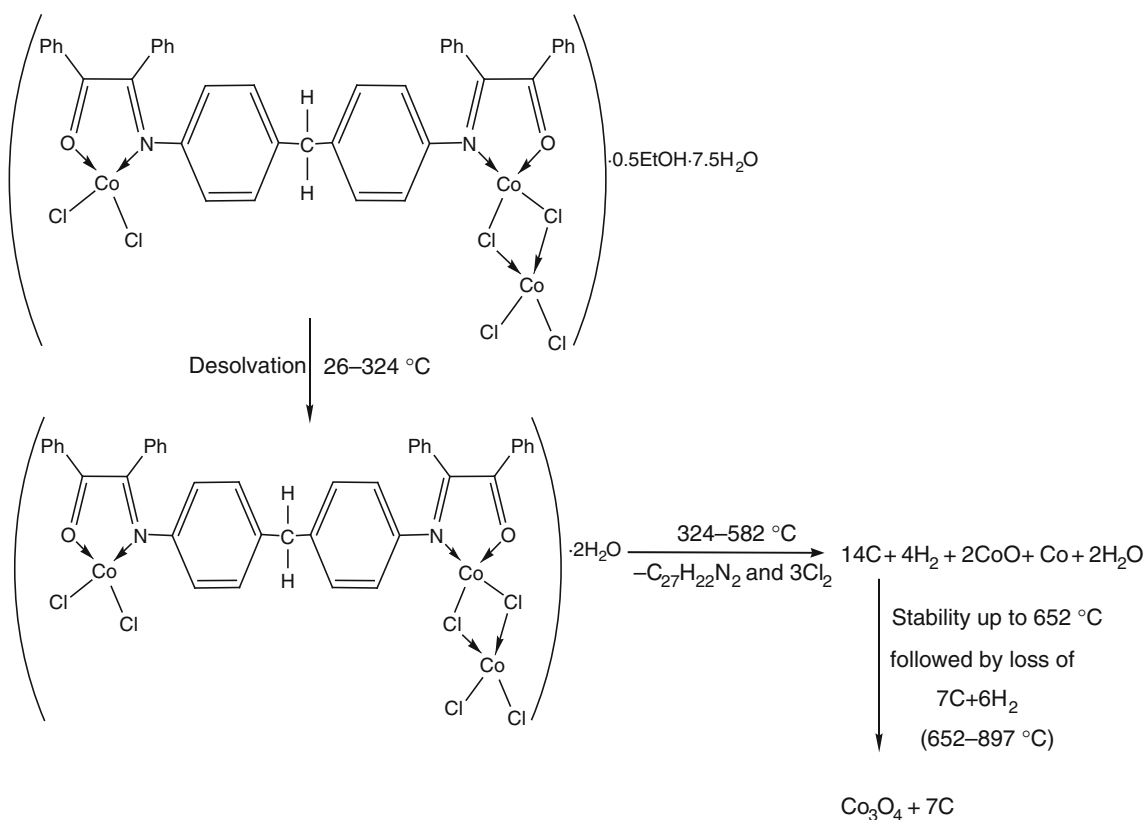
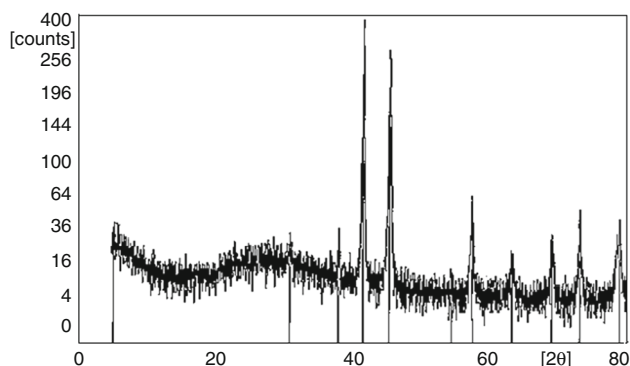**Scheme 4** Proposed thermal decomposition mechanism for Co(II) complex (**1**)

Fig. 9 XRD pattern of CuO as a final product of the thermal decomposition of Cu(II) complex (**6**)

In order to demonstrate the influences of the structural properties of the chelating moiety and the type of the metal ion on the thermal behavior of the metal complexes, the values of activation energy ΔE^* and the order of the reaction for the various decomposition stages were calculated through the analysis of the DTG curves. The reaction order (n) can be determined from the relation [72]:

$$(1 - \alpha_m) = n^{1/1-n}$$

where α_m is the decomposed substance fraction at the maximum development of reaction.

The activation energy (ΔE^*) can be calculated by using the initial rate method [30, 69]. The plot of (ln$I$) versus (1/T) for the low-temperature peak is a straight line with a slop equals to ($-E^*/R$) [70, 71], where I represents the intensity of DTG or DTA peak. Also, the kinetic parameters (ΔH, ΔS^* and ΔG) were calculated using these relations:

$\Delta H = \Delta E^* - RT$; $\Delta S^* = RT \ln(Ah/KT)$; $\Delta G = \Delta H - T\Delta S^*$, where K, h, R, A and T are Boltzmann's, Planck's and gas constants, frequency factor and absolute temperature, respectively.

Considering the TG/DTG curves and kinetic parameters, some remarks and conclusions were obtained as follows:

- The observed higher thermal stability of Ni(II) complex (**2**) (369 °C) than the corresponding for Co(II) complex (**1**) may be ascribed to the increased number of water of crystallization that show vital role in lattice forces [29, 65]. This is because the presence of crystallized water molecules keeps the structure less flexible due to inter- and intrahydrogen bonds [73]. Moreover, the activation energy value of complexes increases as the thermal stability increases. So, ΔE^* value for the initial decomposition for Ni(II) complex (**2**) is higher than that the corresponding ΔE^* for Co(II) complex (**1**), Table 6, and this may be due to the lower ionic radii of Ni(II)
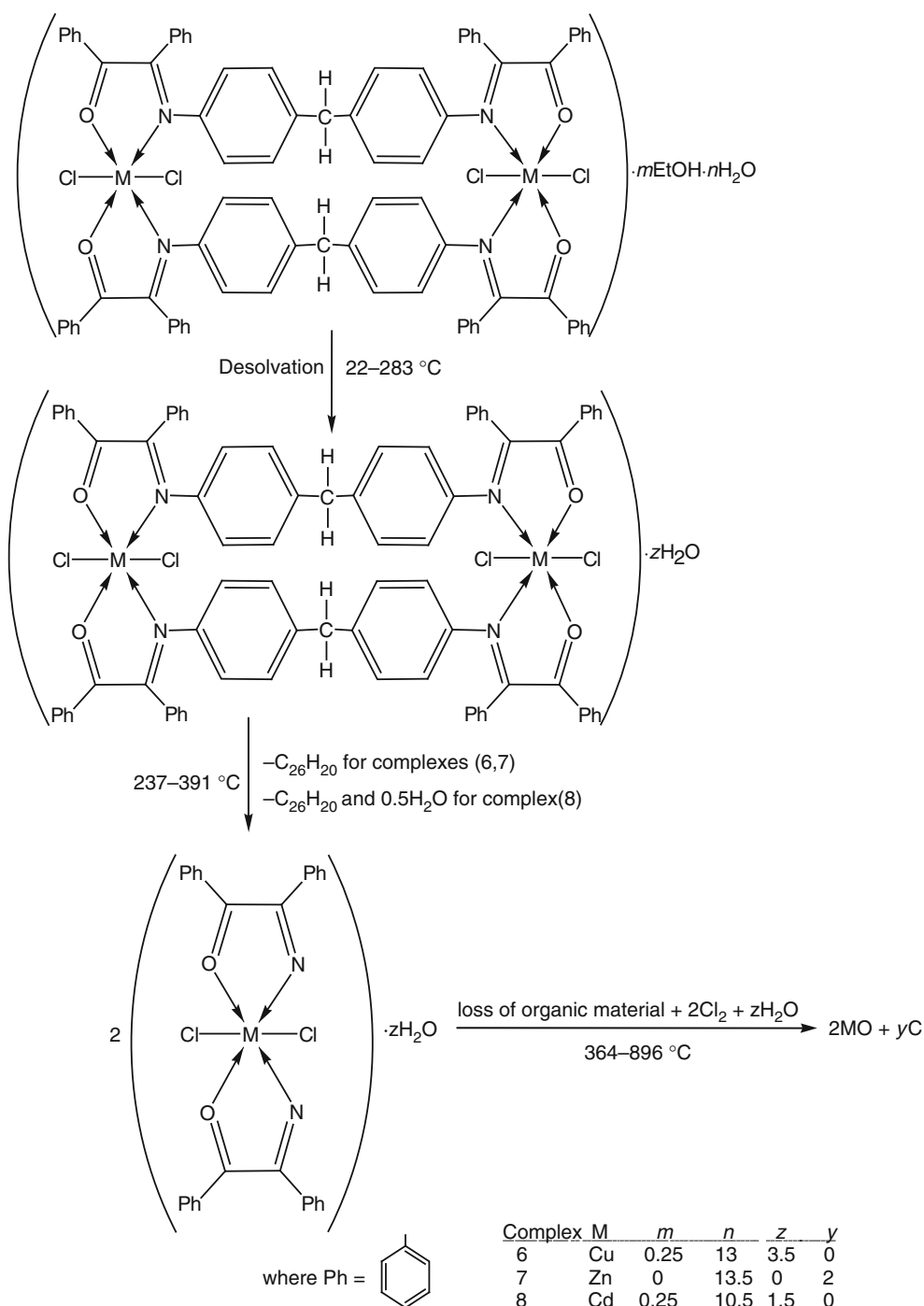
Scheme 5 Thermal decomposition mechanism for Schiff base metal complexes (6–8)

ion than that of Co(II) ion [50, 74]. Also, all the decomposition processes of Ni(II) complex proceed through second-order reaction, whereas Co(II) complex proceeds through first-order reaction (Table 6).

- The higher thermal stability of the octahedral Co(II) complex (4) than the tetrahedral Co(II) complex (1) may be due to the ionic character of complex (4) and

the stronger interaction between Co(II) ion and NO_3Cl_2 chromophore in octahedral Co(II) complex [75]. Also, all the decomposition processes of Co(II) complexes (1,4) occur through first-order reaction (Table 6).

- Sandwich complexes (6–8) are isothermal, while Zn(II) complex (7) has higher thermal stability comparing to Cu(II) (6) and Cd(II) (8) complexes. This may be due to

Table 6 Kinetic and thermodynamic parameters of the thermal decomposition of the Schiff base ligand and its metal complexes

No.	Compound	Temperature range/°C	DTG peak Temperature/°C	n	$\Delta E^*/$ kJ mol^{-1}	$\Delta H^*/$ kJ mol^{-1}	A/s^{-1}	$-\Delta S^*/$ kJ mol^{-1} K^{-1}	$\Delta G^*/$ kJ mol^{-1}
	L	184–270	228[b]	1.31	207.36	203.49	259.33	0.2113	301.76
		270–381	328[a]	1.29	324.16	321.40	340.87	0.2106	391.31
		381–872	660[e]	1.84	250.25	245.59	157.51	0.2206	369.37
1	[Co$_3$(L)Cl$_6$]·0.5EtOH·7.5H$_2$O	26–324	39[c]	1.71	127.71	125.33	271.90	0.2070	184.53
			73[c]	1.29	222.87	220.50	457.13	0.2035	278.51
			166[e]	1.00	111.24	108.46	154.08	0.2146	180.12
		324–582	455[f]	1.22	147.05	143.69	118.48	0.2209	232.95
		652–897	746[b]	1.16	531.52	527.89	315.98	0.2156	622.11
			879[c]	1.03	965.39	962.56	518.88	0.2125	1035.23
2	[Ni$_3$(L)Cl$_6$]·12.25H$_2$O	26–369	43[c]	1.93	102.25	99.84	207.63	0.2093	160.55
		369–588	442[f]	1.87	372.79	370.21	322.91	0.2125	436.29
		588–899	691[c]	1.57	827.92	825.42	542.34	0.2106	888.82
3	[Cu$_3$(L)Cl$_6$]·6H$_2$O	23–222	44[c]	1.71	142.45	140.01	302.32	0.2062	200.65
		222–450	253[a]	1.48	233.98	231.45	279.38	0.2111	295.63
		450–898	332[a]	1.04	278.59	275.92	286.27	0.2121	343.99
			409[c]	0.98	872.15	869.63	970.73	0.2029	931.11
			679[c]	1.10	825.05	820.88	548.55	0.2104	926.52
4	[Co$_3$(L)Cl$_5$(H$_2$O)$_7$]·Cl·4.5EtOH	23–193	39[d]	1.06	220.77	218.18	539.52	0.0202	225.10
			157[b]	0.90	77.74	74.99	107.96	0.0362	90.58
		193–350	333[a]	1.34	189.23	1186.82	1652.07	0.0139	1195.26
		350–561	399[a]	1.78	258.92	1256.24	1487.26	0.0182	1268.44
			509[b]	1.01	588.01	585.44	479.22	0.0288	607.99
		561–899	743[e]	1.33	634.15	631.13	381.53	0.0329	664.56
5	[Ni$_2$(L)Cl$_4$(H$_2$O)$_4$]·2EtOH	25–327	40[d]	2.07	239.91	237.51	584.19	0.0196	243.64
			170[c]	1.05	115.65	112.56	159.10	0.0333	127.31
		327–499	436[f]	1.40	206.98	203.81	174.14	0.0364	229.64
		499–719	517[b]	0.81	731.23	728.81	605.01	0.0269	750.12
			685[d]	1.01	672.45	699.66	435.21	0.0313	699.66
6	[Cu$_2$(L)$_2$Cl$_4$]·0.25EtOH·13H$_2$O	22–237	45[c]	1.77	84.06	81.60	165.85	0.2113	144.14
			164[c]	1.32	778.91	776.60	1652.71	0.1948	831.73
			182[c]	1.17	500.12	497.83	834.41	0.2008	553.25
			203[d]	0.80	963.29	960.95	1915.87	0.1943	1015.74
			220[d]	1.68	527.31	524.97	788.29	0.2020	581.92
		237–391	267[e]	1.32	359.58	357.07	438.48	0.2076	419.76
			360[c]	0.88	462.02	459.33	476.01	0.2082	526.79
		391–703	458[b]	1.12	241.64	238.84	198.16	0.2167	311.87
			666[e]	0.58	558.52	554.85	364.41	0.2137	649.10
7	[Zn$_2$(L)$_2$Cl$_4$]·13.5H$_2$O	25–283	51[c]	1.35	55.14	52.65	102.92	0.0343	63.76
			176[b]	0.84	120.44	117.64	163.63	0.0332	132.53
			254[b]	1.44	717.06	714.35	1053.77	0.0189	724.36
		283–376	358[a]	1.11	622.86	619.97	676.40	0.0242	635.23
		376–675	452[a]	1.90	508.17	505.27	447.00	0.0288	526.14
			610[c]	1.23	687.96	684.87	491.84	0.0296	711.03
			652[c]	0.60	1715.01	1712.66	1339.55	0.0217	1732.73

Table 6 continued

| No.	Compound	Temperature range/°C	DTG peak Temperature/°C	n	ΔE^*/ kJ mol^{-1}	ΔH^*/ kJ mol^{-1}	A/s^{-1}	$-\Delta S^*$/ kJ mol^{-1} K^{-1}	ΔG^*/ kJ mol^{-1}
8	$[Cd_2(L)_2Cl_4]\cdot0.25EtOH\cdot10.5H_2O$	28–277	139[b]	1.11	117.56	114.37	175.94	0.2129	196.13
			245[b]	1.26	231.68	228.86	281.50	0.2109	300.36
		277–364	325[a]	1.18	289.89	287.23	303.18	0.2115	354.91
		364–896	431[a]	1.26	365.71	362.88	322.05	0.2124	435.08
			587[a]	1.32	593.56	590.53	431.23	0.2116	667.76

[a] Strong

[b] Medium

[c] Weak

[d] Very weak

[e] Broad

[f] Broad strong

the decrease in electronegativity of metal ion, where the difference in electronegativity between the metal ion and the donor atoms of the ligand (N and O atoms) will decrease, producing higher ionic character for metal–ligand bond and higher thermal stability for this chelate. In addition, the coordinated Schiff base ligand starts to decompose in the second stage for complexes (**6–8**) and the calculated activation energy values (Table 6) are found to be 359.58, 622.86 and 289.89 kJ mol^{-1}, respectively. This reflects the higher thermal stability of Zn(II) complex which is shown by its high decomposition temperature (283 °C) than that observed for Cu(II) and Cd(II) complexes.

- The change of entropy values (ΔS^*) of complexes (**1–8**) for the thermal decomposition steps (Table 6) showed that the transition states are more ordered, i.e., in a less random molecular configuration than the reacting complexes. Also, the fraction appeared in the calculated order of the thermal reactions (n) confirmed that the reactions proceeded in complicated mechanisms [68].

Electronic spin resonance (ESR) spectral studies

The X-band ESR spectra of Cu(II) complexes (**3**, **6**) were recorded on powder sample at room temperature (Fig. 10). The ESR spectra of those complexes were found to be axially symmetric with two g values, $g^{\parallel} = (2.24, 2.23)$, $g_{\perp} = (2.08, 2.07)$, respectively (Table 7). The observed $g^{\parallel}$ values for these complexes are greater than g_e (2.0023), indicating that $(d_{x2-y2})^1$ is the ground state for Cu(II) ions configuration, i.e., $^4(a_{1g})^2(b_{2g})^2(b_{1g})^1$, which is characterized to square planar or distorted octahedral geometry [77, 78]. The calculated g_{av} values (2.13, 2.12) and the
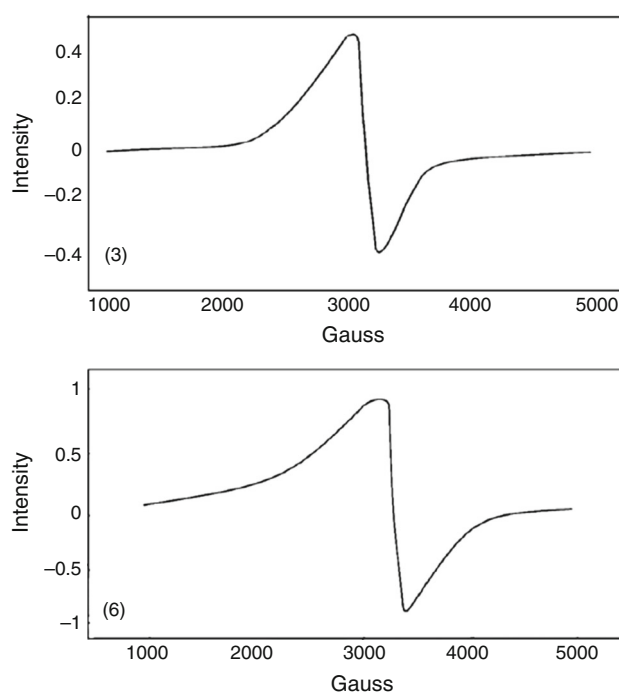
Fig. 10 ESR spectra of $[Cu_3(L)Cl_6]\cdot6H_2O$ (**3**) and $[Cu_2(L)_2Cl_4]$-$0.25EtOH\cdot13H_2O$ (**6**)

Table 7 ESR parameters of the Schiff base copper(II) complexes

Complex	$g^{\parallel}$	$g_{\perp}$	$g_{av.}$	G
(**3**)	2.24	2.08	2.13	3.16
(**6**)	2.23	2.07	2.12	3.36

$g_{av.} = (2\,g_{\perp} + g^{\parallel})/3$

observed $g^{\parallel}$ values (2.24, 2.23), which are <2.3, suggest the high covalent character of metal–ligand bond with distorted symmetry [52–54]. In axial symmetry,

$G = (g^{\parallel} - 2.0023)/(g_{\perp} - 2.0023)$, where G measures the exchange interaction between the metal centers in a polycrystalline solid. The calculated G values for complexes (**3**, **6**) are 3.16 and 3.36, respectively, suggesting the copper–copper exchange interaction in the solid complexes [79]. These results are in agreement with the magnetic moment values for complexes (**3**, **6**) (Table 4).

References

1. Golcu A, Tumer M, Demirelli H, Wheatley RA. Cd(II) and Cu(II) complexes of polydentate Schiff base ligands: synthesis, characterization, properties and biological activity. Inorg Chim Acta. 2005;358:1785–97.

2. Dhahagani K, Kumar SM, Chakkaravarthi G, Anitha K, Rajesh J, Ramu A, Rajagopal G. Synthesis and spectral characterization of Schiff base complexes of Cu(II), Co(II), Zn(II) and VO(IV) containing 4-(4-aminophenyl) morpholine derivatives: antimicrobial evaluation and anticancer studies. Spectrochim Acta A. 2014;117:87–94.

3. Jayabalakrishnan C, Karvembu R. Catalytic and antimicrobial activities of new ruthenium(II) unsymmetrical Schiff base complexes. Transit Met Chem. 2002;27:790–4.

4. Prabhakaran R, Geetha A, Thilagavathi M, Karvembu R, Krishnan V, Bertagnolli H, Natarajan K. Synthesis, characterization, EXAFS investigation and antibacterial activities of new ruthenium(III) complexes containing tetradentate Schiff base. J Inorg Biochem. 2004;98:2131–40.

5. Balasubramanian KP, Karvembu R, Prabhakaran R, Chinnusamy V, Natarajan K. Synthesis, spectral, catalytic and antimicrobial studies of PPh₃/AsPh₃ complexes of Ru(II) with dibasic tridentate O, N, S donor ligands. Spectrochim Acta A. 2007;68:50–4.

6. Sadeek SA, Refat MS. Preparation and characterization of Tin(II) complexes with isomeric series of Schiff bases as ligands. J Korean Chem Soc. 2006;50:107–15.

7. Uddin MN, Abdus Salam Md, Sultana J. Pb(II) complexes of Schiff bases derived from benzoylhydrazine as the antibacterial agents. Mod Chem. 2015;3:7–14.

8. Zhou X, Shao L, Jin Z, Liu J-B, Dai H, Fang J-X. Synthesis and antitumor activity evaluation of some Schiff bases derived from 2-aminothiazole derivatives. Heteroatom Chem. 2007;18:55–9.

9. Plentz Meneghetti S, Kress J, Lutz PJ. Structural investigation of poly(olefin)s and copolymers of ethylene with polar monomers prepared under various reaction conditions in the presence of palladium catalysts. Macromol Chem Phys. 2000;201:1823–32.

10. Saadeh HA, AbuShaireh EA, Mosleh IM, Al-Bakri AG, Mubarak MS. Synthesis, characterization and biological activity of Schiff bases derived from metronidazole. Med Chem Res. 2012;21:2969–74.

11. Luo XF, Hu X, Zhao XY, Goh SH, Li XD. Miscibility and interactions in blends and complexes of poly(4-methyl-5-vinylthiazole) with proton-donating polymers. Polymer. 2003;44:5285–91.

12. Bhkakh CK, Hadi JS. New unsymmetrical Schiff base as inhibitor of carbon steel corrosion and antibacterial activity. Res J Chem Sci. 2015;5:64–70.

13. Gupta AK, Pal R. Dehydroacetic acid based Schiff bases and their metal complexes: a review. World J Pharm Pharmacol Sci. 2015;4:386–425.

14. Parrey IR, Hashmi AA. Synthesis of Schiff base complexes of Mn(II) and Co(II) and their catalytic oxidation towards olefins and alcohols. Can Chem Trans. 2015;3:65–71.

15. Quintana PJE, De Peyster A, Klatzke S, Park HJ. Gossypol-induced DNA breaks in rat lymphocytes are secondary to cytotoxicity. Toxicol Lett. 2000;117:85–94.

16. Yadav G, Mani JV. Green synthesis of Schiff bases by using natural acid catalysts. Int J Sci Res. 2015;4:121–7.

17. Maxim C, Pasatoiu TD, Ch Kravtsov V, Shova S, Muryn CA, Winpenny REP, Tuna F, Andruh M. Copper(II) and zinc(II) complexes with Schiff-base ligands derived from salicylaldehyde and 3-methoxysalicylaldehyde: synthesis, crystal structures, magnetic and luminescence properties. Inorg Chim Acta. 2008;361:3903–11.

18. Patel IJ, Parmar SJ. Synthesis and studies of novel optically active Schiff base derivatives and their antimicrobial activities. E J Chem. 2010;7:617–23.

19. Charef N, Sebti F, Arrar L, Djarmouni M, Boussoualim N, Baghiani A, Khennouf S, Ourari A, AlDamen MA, Mubarak MS, Peters DG. Synthesis, characterization, X-ray structures, and biological activity of some metal complexes of the Schiff base 2,2′-((azanediylbis(propane-3,1-diyl))bis(azanylylidene))bis(methanylylidene) diphenol. Polyhedron. 2015;85:450–6.

20. Asadi Z, Asadi M, Setoodehkhah M. Thermodynamics of adduct formation of cobalt(II) tetraaza Schiff base complexes with organotin(IV) trichlorides. Spectrochim Acta A. 2013;112:214–8.

21. Carlsson H, Haukka M, Bousseksou A, Latour JM, Nordlander E. Nickel complexes of carboxylate-containing polydentate ligands as models for the active site of urease. Inorg Chem. 2004;43:8252–62.

22. Kang S-G, Song J, Jeong JH. Synthesis and characterization of new unsaturated macrobicyclic and bis(macrocyclic) copper(II) complexes containing N–CH2–N linkages. Inorg Chim Acta. 2004;357:605–10.

23. Mizuno M, Iwata K, Takahashi H. Time-resolved infrared and resonance Raman studies of benzyl, vibrational analysis and structures of the excited states. J Mol Struct. 2003;661–662:3–10.

24. Singh D, Kumar K, Kumar R, Singh J. Template synthesis and characterization of biologically active transition metal complexes comprising 14-membered tetraazamacrocyclic ligand. J Serb Chem Soc. 2010;75:217–28.

25. Bassett J, Denney RC, Jeffery GH, Mendham J. Vogel's textbook of quantitative inorganic analysis including elementary instrumental analysis. 4th ed. London: Longman Group; 1978.

26. Lewis J, Wilkins RG. Modern coordination chemistry. New York: Interscience; 1960. p. 403.

27. Saikat S, Kumar NS, Prasun CA, Kamalendu D. Synthesis and spectroscopic characterization of some Iron(III) complexes with tetradentate Schiff base ligands. Ind J Sci. 2015;12:17–24.

28. Mahal A, Abu-El-Halawa R, Zabin SA, Ibrahim M, Al-Refai M, Kaimari T. Synthesis, characterization and antifungal activity of some metal complexes derived from quinoxaloylhydrazone. World J Org Chem. 2015;3:1–8.

29. AbouEl-Enein SA. Polymeric and sandwich Schiff's bases complexes derived from 4,4′-methylenedianiline; characterization and thermal investigation. J Therm Anal Calorim. 2008;91:929–36.

30. AbouEl-Enein SA, Emam SM, Polis MW, Emara EM. Synthesis and characterization of some metal complexes derived from azo compound of 4,4′-methylenedianiline and antipyrine: evaluation of their biological activity on some land snail species. J Mol Struct. 2015;1099:567–78.

31. Ubani OC, Oforka NC, Ngochindo RI, Odokuma LO. Synthesis, characterization and antimicrobial studies of cinnamaldehyde benzylamine Schiff base metal ion complexes. Res J Chem Sci. 2015;5:14–22.

32. Mary YS, Panicker CY, Sapnakumari M, Narayana B, Sarojini BK, Al-Saadi AA, Alsenoy CV, War JA, Fun HK. Infrared spectrum, structural and optical properties and molecular docking study of 3-(4-fluorophenyl)-5-phenyl-4,5-dihydro-1H-pyrazole-1-carbaldehyde. Spectrochim Acta A. 2015;138:529–38.

33. Lad HB, Giri RR, Chovatiya YL, Brahmbhatt DI. Synthesis of modified pyridine and bipyridine substituted coumarins as potent antimicrobial agents. J Serb Chem Soc. 2015;80:1–21.

34. Anacona JR, Noriega N, Camus J. Synthesis, characterization and antibacterial activity of a tridentate Schiff base derived from cephalothin and sulfadiazine, and its transition metal complexes. Spectrochim Acta A. 2015;137:16–22.

35. Tripathy SK, Panda A, Das PK, Behera NK, Mahapatra A, Panda AK. Homo and bimetallic dinuclear macrocyclic complexes of 1,4,5, 8,11,14,15,18,19,21, decaaza-2,3,6,7,12,13,16,17,-octaphenyl-20-thia-undodecane1,3,5,7,11,13,15,17-octaene-(dotuo): its synthesis, characterization and biological properties. Int J Sci Environ Technol. 2014;3:208–23.

36. Singh VP, Gupta P, Lal N. Synthesis, spectral, and biological studies of some metal(II) complexes with benzil salicylaldehyde acyldihydrazones. Russ J Coord Chem. 2008;34:270–7.

37. Raman N, Ravichandran S, Thangaraja C. Copper(II), cobalt(II), nickel(II) and zinc(II) complexes of Schiff base derived from benzil-2,4-dinitrophenylhydrazone with aniline. J Chem Sci. 2004;116:215–9.

38. Jha A, Murthy YLN, Durga G. Synthesis, characterization and bioactivity of transition metal complexes of new 3-methyl-5-mercapto-4-triazole Schiff bases. Res J Pharm Biol Chem Sci. 2015;6:1306–14.

39. Anitha C, Sheela CD, Tharmaraj P, Sumathi S. Spectroscopic studies and biological evaluation of some transition metal complexes of azo Schiff-base ligand derived from (1-phenyl-2,3-dimethyl-4-aminopyrazol-5-one) and 5-((4-chlorophenyl)diazenyl)-2-hydroxy-benzaldehyde. Spectrochim Acta A. 2012;96:493–500.

40. Tyagi P, Chandra S, Saraswat BS. Ni(II) and Zn(II) complexes of 2-((thiophene-2-ylmethylene)amino)benzamide: synthesis, spectroscopic characterization, thermal, DFT and anticancer activities. Spectrochim Acta A. 2015;134:200–9.

41. Abd-Elzaher MM, Shakdofa MME, Mousa HA, Moustafa SA. Synthesis, characterization and biological activity of some ferrocenyl complexes containing antipyrine moiety. SOP Trans Appl Chem. 2014;1:42–52.

42. Kumar DS, Gandhi SR, Sheriff AKI. Synthesis, spectral characterization and antimicrobial activity of bidentate Schiff's base (N2) transition metal complexes. J Chem Pharm Res. 2015;7:416–23.

43. Masoud MS, El-Marghany A, Orabi A, Ali AE, Sayed R. Spectral, coordination and thermal properties of 5-arylidene thiobarbituric acids. Spectrochim Acta A. 2013;107:179–87.

44. Allinger NL. Conformational analysis. 130. MM2. A hydrocarbon force field utilizing V1 and V2 torsional terms. J Am Chem Soc. 1977;99:8127–34.

45. Zimmer M. Bioinorganic molecular mechanics. Chem Rev. 1995;95:2629–49.

46. Hay BP, Hancock RD. The role of donor group orientation as a factor in metal ion recognition by ligands: review article. Coord Chem Rev. 2001;212:61–78.

47. Salavati-Niasari M, Davar F, Saberyan K. Template synthesis and characterization of diazadioxa macrocyclic nanosized cobalt(II) complex dispersed within nanocavity of zeolite-Y. Polyhedron. 2010;29:2149–56.

48. El-Gammal OA, Elmorsy EA, Sherif YE. Evaluation of the anti-inflammatory and analgesic effects of Cu(II) and Zn(II) complexes derived from 2-(naphthalene-1-yloxy)-N′-(1-(pyridin-2-1)ethylene)acetohydrazide. Spectrochim Acta A. 2014;120:332–9.

49. Bagdatli E, Gunkara OT, Ocal N. Synthesis and characterization of new copper(II) and palladium(II) complexes with azo-, bisazo-5-pyrazolones. J Organomet Chem. 2013;740:33–40.

50. El-Sonbati AZ, Diab AA, El-Bindary AA, El-Desoky AM, Morgan ShM. Correlation between ionic radii of metals and thermal decomposition supramolecular structure of azodye complexes. Spectrochim Acta A. 2015;135:774–91.

51. Abdallah SM, Mohamed GG, Zayed MA, Abou El-Ela MS. Spectroscopic study of molecular structures of novel Schiff base derived from o-phthalaldehyde and 2-aminophenol and its coordination compounds together with their biological activity. Spectrochim Acta A. 2009;73:833–40.

52. El-Boraey HA, Emam SM, Tolan DA, El-Nahas AM. Structural studies and anticancer activity of a novel (N_6O_4) macrocyclic ligand and its Cu(II) complexes. Spectrochim Acta A. 2011;78:360–70.

53. Gupta OP, Kumar A. Metal complexes as ligand: binuclear Ni(II) and Cu(II) metal chelates of p-methylisonitrosoacetophenone with alkali metal salts. J Chem Chemic Sci. 2015;5:69–78.

54. Hasanvand F, Ahmadi RA, Amani S. Synthesis, spectroscopy and magnetic characterization of five dinuclear copper(II) complexes with 2, 3 or 4-pyridinemethanol as the ligand. J Sci. 2012;23:37–43.

55. El-Ayaan U, Kenawy IM, Abu El-Reash YG. Synthesis, thermal and spectral studies of first-row transition metal complexes with girard P reagent-based ligand. Spectrochim Acta A. 2007;68:211–9.

56. Lever ABP. Inorganic electronic spectroscopy. Amsterdam: Elsevier; 1968. p. 249–372.

57. Gaber M, El-Hefnawy GB, El-Borai MA. Synthesis, spectral and thermal studies of Mn(II), Co(II), Ni(II), Cu(II) and Zn(II) complexes dyes based on hydroxyquinoline moiety. J Therm Anal Calorim. 2012;109:1397–405.

58. Ur-Rehman S, Ikram M, Rehman S, Ul Islam N, Jan N. Synthesis and characterization of Ni(II), Cu(II) and Zn(II) tetrahedral transition metal complexes of modified hydrazine. J Mex Chem Soc. 2011;55:164–7.

59. Chohan ZH, Arif M, Akhtar MA, Supuran CT. Metal-based antibacterial and antifungal agents: synthesis, characterization, and in vitro biological evaluation of Co(II), Cu(II), Ni(II) and Zn(II) complexes with amino acid-derived compounds. Bioinorg Chem Appl. 2006;2006:1–13.

60. El-Tabl AS, AbouEl-Enein S. Reactivity of the new potentially binucleating ligand, 2-(acetichydrazido-N-methylidene-α-naphthol)-benzothiazol, towards manganese (II), nickel (II), cobalt (II), copper (II) and zinc (II) salts. J Coord Chem. 2004;57:281–94.

61. Emam SM, El-Table AS, Ahmed HM, Emad EA. Synthesis, structural characterization, electrochemical and biological studies on divalent metal chelates of a new ligand derived pharmaceutical preservative: dehydroacetic acid with 1,4-diaminobenzene, Arab J Chem. 2014. (**in press**).

62. Jupta LK, Banssal U, Chandra S. Spectroscopic and physicochemical studies on nickel (II) complexes of isatin-3,2′-quinolylhydrazones and their adducts. Spectrochim Acta A. 2007;66:972–5.

63. Leka ZB, Leovac VM, Lukić S, Sabo TJ, Trifunović SR, Szécsényi KM. Synthesis and physicochemical characterization of new dithiocarabamato ligand and its complexes with copper (II), nickel (II) and palladium (II). J Therm Anal Calorim. 2006;83:687–91.

64. Rosu T, Pahontu E, Maxim C, Georgescu R, Stanica N, Almajan GL, Gulea A. Synthesis, characterization and antibacterial activity of some new complexes of Cu(II), Ni(II), VO(II), Mn(II) with Schiff base derived from 4-amino-2,3-dimethyl-1-phenyl-3-pyrazolin-5-one. Polyhedron. 2010;29:757–66.

65. Emam SM, El-Sayed IE, Nassar N. Transition metal complexes of neocryptolepine analogues, Part I: synthesis, spectroscopic characterization, and in vitro anticancer activity of copper (II) complexes. Spectrochim Acta A. 2015;138:942–53.

66. El-Metwally NM, Arafa R, El-Ayaan U. Molecular modeling, spectral, and biological studies of 4-formylpyridine-4N-(2-pyridyl)thiosemicarbazone (HFPTS) and its Mn(II), Fe(III), Co(II), Ni(II), Cu(II), Cd(II), Hg(II), and UO$_2$(II) complexes. J Therm Anal Calorim. 2014;115:2357–67.

67. Stefanescu O, Vlase T, Sorescu S. Thermal behavior of Co(II) and Ni(II) hydroxycarboxylate complexes obtained by two original synthesis methods. J Therm Anal Calorim. 2013;113:1345–54.

68. M.S. Masoud, S.A. Abou El-Enein, A.M. Ramadan, A.S. Goher, (2008) Thermal properties of some biologically active 5-(p-substituted phenylazo)-6-aminouracil complexes. J Anal Appl Pyrolysis 2008;81:45-51

69. Kirsh Y, Yariv S, Shoval S. Kinetic analysis of MgCl$_2$·6H$_2$O by DTA and DTG. J Therm Anal Calorim. 1987;32:393–408.

70. Piloyan GO, Ryabchikov ID, Novikova OS. Determination of activation energies of chemical reactions by differential thermal analysis. Nature. 1966;212:1229.

71. Alaghaz AMA, Zayed ME, Alharbi SA, Ammar RAA. Synthesis, spectroscopic identification, thermal, potentiometric and antibacterial activity studies of 4-amino-5-mercapto-S-triazole Schiff's base complexes. J Mol Struct. 2015;1087:60–7.

72. Ostwald HF, Dubler E. In: Wiedemann HG, editor. Thermal analysis, vol. 2. Inorganic Chemistry/Metallurgy/Earth Sciences. Basel: Switzerland Birkhauser; 1972.

73. Baran Y, Kaya I, Turkyilmaz M. Synthesis, spectroscopic and thermal properties of Pt(II) complexes of some polydentate ligands. J Therm Anal Calorim. 2012;107:809–75.

74. Breviglieri ST, Cavalheiro ETG, Chierice GO. Correlation between ionic radius and thermal decomposition of Fe(II), Co(II), Ni(II), Cu(II) and Zn(II) diethanoldithiocarbamates. Thermochim Acta. 2000;356:79–84.

75. Mahmoud MA, Zaitone SA, Ammar AM, Sallam SA. Synthesis, structure and antidiabetic activity of chromium (III) complexes of metformin Schiff bases. J Mol Struct. 2016;1108:60–70.

76. Masoud MS, Ali AE, Ghareeb DA, Nasr NM. Structural, spectral and thermal analysis of some metallocephradine. J Mol Struct. 2015;1099:359–72.

77. Tyagi P, Chandra S, Saraswat BS, Yadav D. Design, spectral characterization, thermal, DFT studies and anticancer cell line activities of Co(II), Ni(II) and Cu(II) complexes of Schiff bases derived from 4-amino-5-(pyridin-4-yl)-4H-1,2,4-triazole-3-thiol. Spectrochim Acta A. 2015;145:155–64.

78. Chandra S, Bargujar S, Nirwal R, Yadav N. Synthesis, spectral characterization and biological evaluation of copper(II) and nickel(II) complexes with thiosemicorbazone derived from a bidentate Schiff base. Spectrochim Acta A. 2013;106:91–8.

79. Hathaway BJ, Bardley JN, Gillard RD, editors. Essays in chemistry. New York: Academic Press; 1971.